Chapter 2

Regulating Drug Efficacy by Topological Distribution of N–H···O and O–H···O Interactions in Dimorphic Famotidine Molecular Salts

2.1 Abstract

Crystallization of antiulcer drug famotidine (FAM) with *ortho*-aminobenzoic acid (2-ABA) in methanol and ethanol affords dimorphic molecular salt hydrates. Both forms are ionic and monohydrates with noticeable differences in the orientation of the water molecule of crystallization leading to variations in intermolecular interactions. The topological distributions for N–H···O and O–H···O hydrogen bonding interactions accessible from the water molecules of crystallization have been identified as the key reason for the alteration of drug efficacy in the multicomponent dimorphic systems. The stability of the structures is due to the ancillary hydrogen bonding estimated in the dimorphic phases of the drug FAM with 2-ABA. The qualitative and quantitative contribution of weak interactions established an agreeable correlation with the measured properties viz. solubility and membrane permeability of the two forms at physiological pH conditions. The strength and distributions for N–H···O and O–H···O along with auxiliary hydrogen bonding, and solute-solvent interactions have shown colossal impact on the drug properties and that too between the polymorphic phases in multicomponent crystals and are emphasized.

2.2 Introduction

Multicomponent crystals such as salts and cocrystals have been widely used to optimize the physicochemical properties of pharmaceutical materials [1–9]. The selection of a coformer for the multicomponent solids formulation is based on the compatibility of its functional groups to form robust supramolecular heterosynthons with the target drug molecule [10–12]. The presence of multiple hydrogen bond donors and acceptors in the drug and coformer molecules offers synthon competition. Such supramolecular synthon competition and conformational variation can give rise to the formation of multicomponent crystal polymorphs as well as variable stoichiometry cocrystals/salts [13,14]. The occurrence of multicomponent crystal polymorphs and variable stoichiometry cocrystals/salts increases the chance to assimilate more solid forms with better efficacy and understanding the existence of such solid phases is extremely important concerning

purity and intellectual property (IP) protection [15–21]. For instance, the anti-inflammatory drug ethenzamide exhibited trimorphic cocrystal structures with 2,4-dihydroxybenzoic acid [1:1 ratio]. The crystal structures of two forms (form I and form III) were determined by single crystal X-ray diffraction. The drug and coformer molecules in Form-I sustained by amide···OH heterosynthon and COOH···COOH homosynthon, whereas Form-III displays amide···COOH and amine···OH heterosynthons [15]. Nangia et al. reported two cocrystal polymorphs of the antibiotic drug sulfacetamide with acetamide in which the metastable Form-I displays a faster dissolution rate than the stable Form-II [16]. The difference in the dissolution rate of three cocrystal polymorphs of the drug ethenzamide with 2,5-dihydroxybenzoic acid was demonstrated [17]. Jones et al. reported physical stability disparity in two cocrystal polymorphs of caffeine with glutaric acid. Form-II exhibits high resistance to hydration in high relative humidity environments as compared to Form-I [18]. The role of hydrogen bonding synthons on the physicochemical properties of various stoichiometric cocrystals of the drug theophylline with 2-ABA was also reported [9]. Solvates of furosemide with DMSO and DMF display dimorphic structures that differ in the conformation of the furosemide molecule and the arrangement of the solvent molecules [22]. The late-stage arrival and consequences of single-component polymorphism in pharmaceutical developments in terms of properties alteration are fairly explored and recognized [23]. However multicomponent crystal polymorphism is still in prologue and largely focuses on the development of crystallization methods, characterization, and evaluation of physicochemical properties. A recent survey on the Cambridge Structural Database (CSD) showed only 184 polymorphic cocrystals and 2539 polymorphic compounds [24].

In this chapter, the synthesis of dimorphic molecular salts of the drug famotidine with *ortho*-aminobenzoic acid is discussed. The role of different hydrogen bond synthons in the stability, solubility, and membrane permeation behaviour of dimorphic molecular salts is illustrated. Famotidine is widely used in the therapy of peptic ulcers and has two polymorphs that vary in their prime hydrogen bond synthons and conformations, i.e., stable Form A and metastable Form B [25–27]. It has low bioavailability and rapidly degrades in acidic conditions. The existence of multiple hydrogen bonding functional groups [i.e. guanidine, amidine, sulphonamide, and thiazole moieties] and the high torsion flexibility of drug molecules can facilitate the occurrences of different polymorphs. New dimorphic salts of FAM with 2-ABA are successfully isolated from the solution

crystallization of ground material in methanol and ethanol (Scheme 2.1). Single crystal structures of both products are determined and found that the orientation of water molecules of crystallization plays a key role in the crystal formation of these polymorphs. The phase purity of new solid products is analysed by vibrational spectroscopy, differential scanning calorimetry, and powder X-ray diffraction. The phase stability, solubility, and membrane permeability of these polymorphs are evaluated in simulated physiological pH conditions.

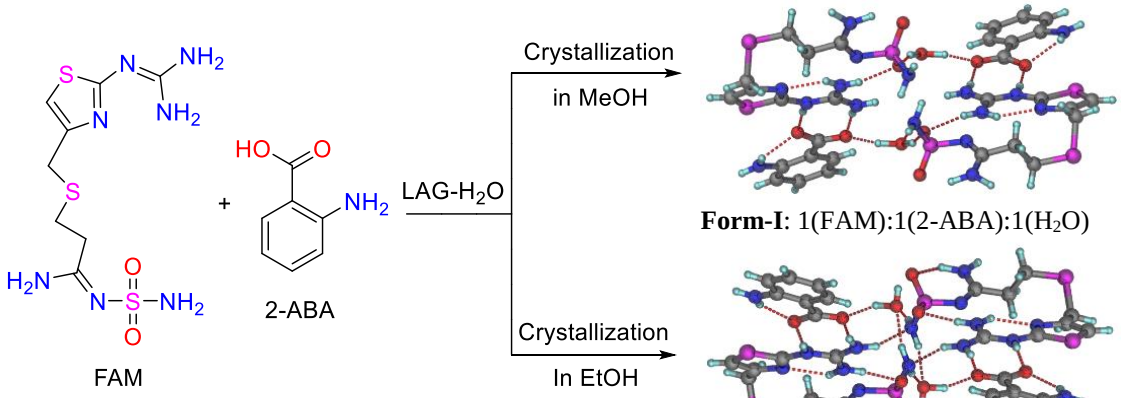

Scheme 2.1 Synthesis of dimorphic salts from API famotidine and 2-aminobenzoic acid.

2.3 Results and Discussion

2.3.1 Synthesis of Molecular Salt and Isolation of Polymorphs

2-aminobenzoic acid (2-ABA) is selected as a coformer to synthesize multicomponent crystals with famotidine (FAM). The starting materials are co-grinded in an equivalent stoichiometric ratio and new distinct two solid phases are isolated from the solution crystallization of ground powder materials (Scheme 2.1). This study illustrates the role of the topological distribution of different hydrogen bonding interactions in tailoring stability, solubility, and membrane permeability of multicomponent crystals of famotidine with 2-ABA compared to pure famotidine. The formulation of multicomponent polymorphs to modulate the physicochemical properties of famotidine targets to achieve the following objectives, (i) to generate new multicomponent polymorphs via solution crystallization method, (ii) to obtain new solid dosage of famotidine that can tolerate even high acidic conditions, (iii) to measure solubility and membrane permeation of the

polymorphs to estimate the in vivo bioavailability of the drug, and (iv) to study the role of various intermolecular interactions in regulating drug properties.

2.3.2 Characterization of Product Phases

Vibrational Spectroscopy (FT-IR). Preliminary analysis of the dimorphic salts of the drug is carried out using FT-IR. It is one of the useful techniques for analyzing hydrogen bond formation in multicomponent systems. The IR stretching frequencies of the dimorphic phases are presented in Figure 2.1 with the comparison of vibrational spectra of that of parent components. The substantial change in the IR spectra indicates the formation of hydrogen bonds between FAM and 2-ABA. The appearance of a new sharp peak around 1400 cm^{-1} notifies proton transfer from 2-ABA to drug FAM. The two new solid forms display similar patterns of peaks in the N–H stretching region, but exhibit some differences in the fingerprint region of the IR absorption spectra.

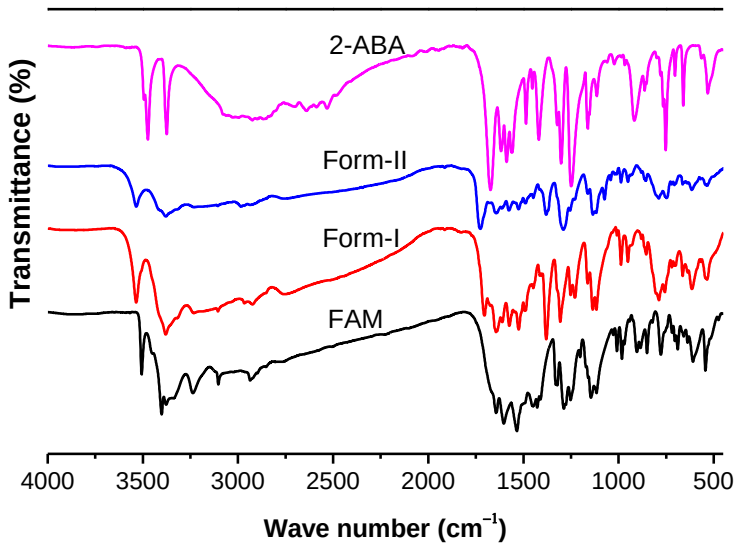

Figure 2.1. The comparison of IR spectra of the dimorphic forms and the starting materials.

Differential Scanning Calorimetry (DSC). The DSC thermal analysis of the dimorphic phases of the salt of FAM and 2-ABA was performed in the temperature range of 25–250 °C. The endothermic onsets of both polymorphs are distinct from the starting components and each other. The observed melting onset temperature for Form-I and Form-II are ~130 and ~116 °C respectively. The loss of solvent molecules in a temperature range that starts at 82 °C for Form-I and 75 °C for Form-II, indicates the presence of water molecules in the crystal lattice of both polymorphs (Figure 2.2). The observed melting temperatures of the two solid materials suggest that Form-I is thermally more stable than Form-II.

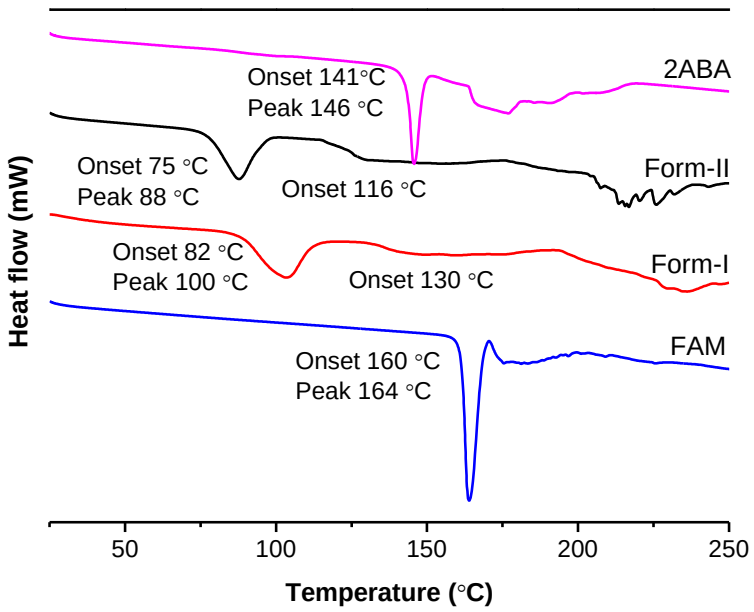

Figure 2.2. DSC endothermic profiles for dimorphic salts and their starting materials.

Thermogravimetric Analysis (TGA). The TGA plots also indicate the presence of water molecule of crystallization in these polymorphs. The weight loss observed for Form-I (obs 3.42%) and Form-II (obs 3.54%) below 120 °C agrees well with the calculated by the single crystal X-ray analysis (Calcd 3.66%), suggesting a monohydrate structure for both polymorphic forms (Figure 2.3).

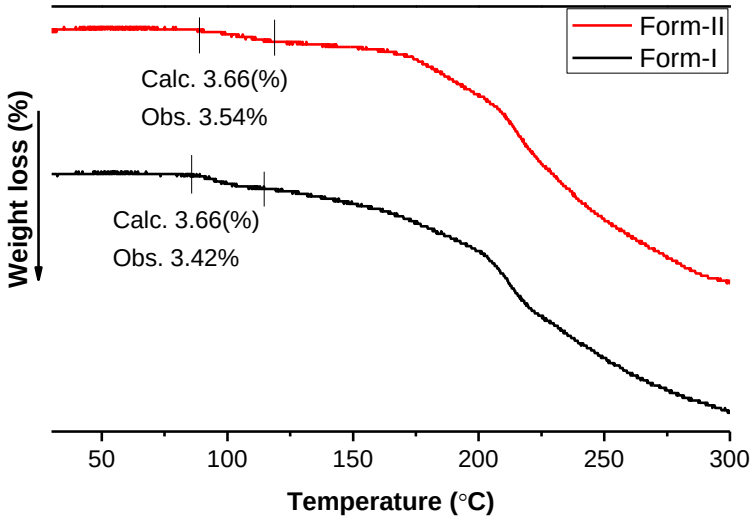

Figure 2.3. The observed TGA weight loss matches well with a 1:1:1 ratio of FAM, 2-ABA, and water estimated by single crystal X-ray structure analysis.

Powder X-ray Diffraction (PXRD). The PXRD pattern and peak positions of Form-II are different from the starting materials, and Form-I, indicating the formation of a new solid phase. The purity of the products is evaluated by comparing the experimental PXRD

patterns with their respective simulated PXRD extracted from their single crystal X-ray structures. The Rietveld refinement shows that the experimental PXRD agrees well with the simulated PXRD, indicating the formation of a pure phase (Appendix Figure A1). The comparison of PXRD patterns of the dimorphic forms shows a noticeable difference in some of the major peak positions. The peaks at 2θ values of 22.48, 26.68, and 27.97° for Form-I and 27.06 and 31.56° for Form-II indicate the difference of the peaks between the two forms and the formation of dimorphic forms Form-I and Form-II (Figure 2.4).

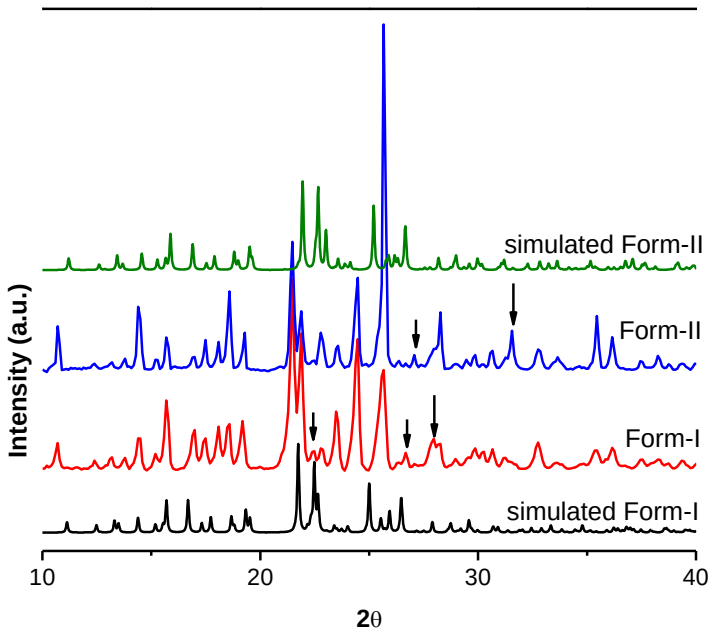

Figure 2.4. The comparison of PXRD patterns of dimorphic forms.

Single Crystal X-RD. The structural variation in the multicomponent polymorphs mainly arises from the differences in the intermolecular interactions (synthon polymorphs) and/or variation in molecular conformation and packing (conformation and packing polymorphs) [13,14]. To understand the molecular packing behavior, hydrogen bonding, and other intermolecular interactions, single crystal X-ray data for both forms are examined. The summary of crystal data parameters is available in Appendix Table A1 and the hydrogen bond geometry is presented in Table 2.1.

Form-I: Isolated Form-I crystal from methanol was solved and refined in an orthorhombic $P2_12_12_1$ space group in a 1:1:1 ratio of FAM, 2-ABA, and water. The guanidine moiety of FAM and COOH group of 2-ABA form $R_2^2(8)$ heterodimer ring motif via N–H···O and N^+–H···O^- interactions as a prime synthon in the crystal structure of Form-I. The intramolecular hydrogen bond is formed from the NH_2 group to the oxygen atom of the carboxylic acid group of the 2-ABA. The water molecule of crystallization is involved in

connecting three dimers through hydrogen bonds to form a molecular tape (Figure 2.5a). The structure extends in 2D via hydrogen bonds from the amine group of amidine moiety to the N-atom of the amine group of the 2-ABA molecule (Figure 2.5b).

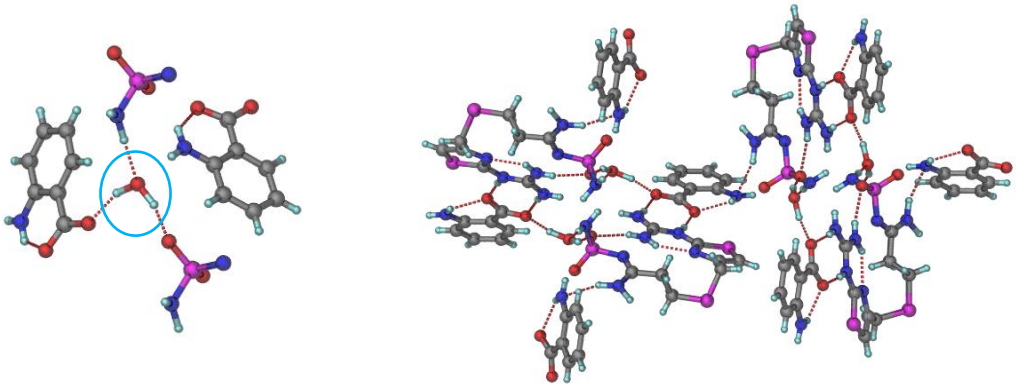

(a) (b)

Figure 2.5 (a) The water molecule serves as a linker between three dimers in the crystal structure of Form-I through auxiliary O–H···N and N–H···O hydrogen bonds. (b) 2D packing of Form-I.

Form-II: The crystals of Form-II were obtained from ethanol and the crystal data was resolved in orthorhombic with a space group of $P2_12_12_1$ with a 1:1:1 ratio of the FAM, 2-ABA, and water. The structure of Form-II also shows the same guanidine···carboxylate prime synthon which is observed in Form-I. The NH_2 group forms an intramolecular interaction with the COOH group in the 2-ABA. Here, the water molecule of crystallization serves as a bridge by connecting four dimers via hydrogen bonds to form a molecular tape (Figure 2.6a). The NH_2 group of 2-ABA is hydrogen bonded with water and the amine group of amidine moiety extends the structure in 2D (Figure 2.6b).

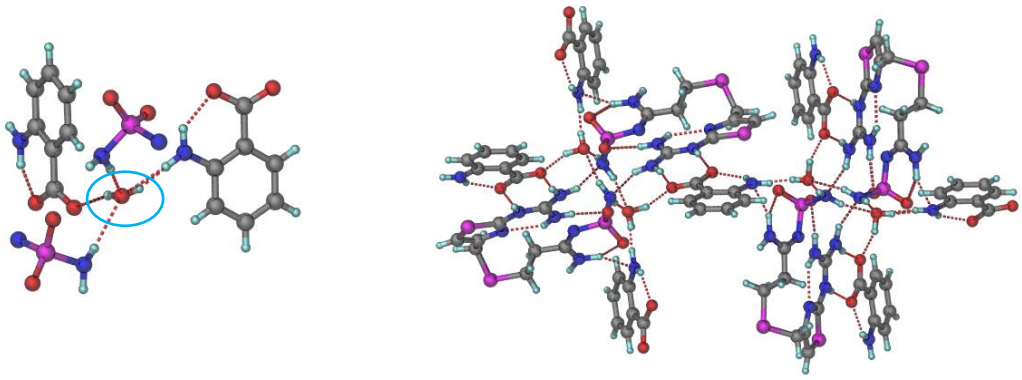

(a) (b)

Figure 2.6 (a) The water molecule connects four dimers in the crystal structure of Form-II via auxiliary O–H···N and N–H···O hydrogen bonds and (b) the 2D structure of Form-II patterns along the crystallographic line [100].

The single crystal structural analysis shows that the two structures vary in the intermolecular interaction patterns, especially in the hydrogen bonds that link the water molecule of crystallization with the FAM and 2-ABA molecules (Figures 2.5a and 2.6a). Essentially the topological distribution of N–H···O and O–H···O interactions played a key role in this dimorphic FAM salt system. The orientation of water molecules in both structures is different (Figures 2.5b and 6b). However, the overlaid conformers of both the drug and coformer extracted from the crystal structures of the polymorphs don't show a clear difference (Figure 2.7).

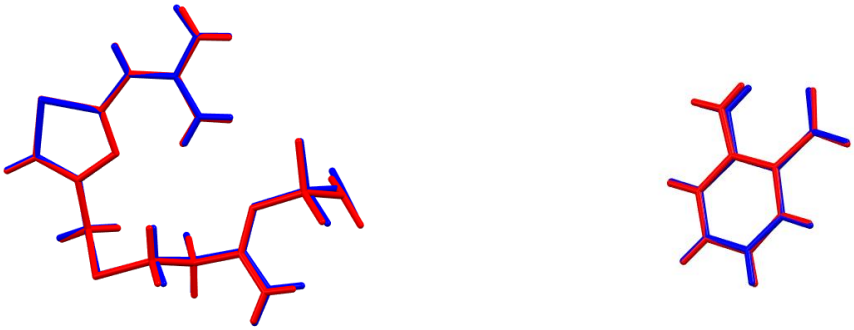

(a) (b)

Figure 2.7. The overlay of molecular conformers (a) drug FAM and (b) 2-ABA extracted from the crystal structures of Form-I and II.

Table 2.1 Important hydrogen bond geometry observed in Form-I and II.

Forms	Interaction	H···A (Å)	D···A (Å)	∠D–H···A (°)	symmetry code
Form-I	N_3–H_{3A}···O_3	1.67	2.700(9)	174	–1/2 – x, 1 – y, –1/2 + z
	N_1–H_{1A}···O_4	1.75	2.775(8)	170	–1/2 – x, 1 – y, –1/2 + z
	O_5–H_{5E}···O_1	1.85	2.797(8)	160	x, y, −1 + z
	O_5–H_{5F}···O_4	1.76	2.687(8)	155	–x, 1/2 + y, 1/2 – z
	N_7–H_{7D}···O_5	1.94	2.970(10)	170	1 + x, y, 1 + z
	N_7–H_{7C}···O_5	2.35	3.300(10)	151	½ + x, 3/2 – y, 1 – z
	N_8–H_{8B}···O_5	2.08	3.104(8)	171	
Form-II	N_3–H_{3A}···O_3	1.77	2.776(4)	163	x – 1, y, z
	N_1–H_{1A}···O_4	1.77	2.793(5)	168	x – 1, y, z
	N_7–H_{7D}···O_5	1.85	2.523(4)	173	3/2 + x, 1/2 – y, 1 – z
	N_8–H_{8B}···O_5	1.85	2.887(5)	176	1 – x, 1/2 + y, 3/2 – z
	N_2–H_{2A}···O_1	1.96	2.960(5)	160	
	O_5–H_{5F}···O_4	1.81	2.752(5)	159	-1 + x, y, z
	O_5–H_{5F}···N_8	1.97	2.880(5)	153	1 – x, 1/2 + y, 3/2 – z
	N_7–H_{8c}···O_5	2.07	3.022(5)	151	½ + x, ½ – y, 1 – z

Hirshfeld surface analysis. Generally, a Hirshfeld surface is a fingerprint for given crystal material and gives important insights into its crystal structure. The 2D fingerprint plots have been used to study polymorphism [28–31]. The X-Seed diagrams in Figures 2.5 and 6 show the major hydrogen bonding interaction differences within the two crystal structures of the molecular salt. The Hirshfeld surface analysis was carried out for both solid forms to analyze the hydrogen bonding interactions difference quantitatively and understand how the variation of such interactions regulates the physicochemical properties of the drug. The 2D fingerprint plots of different hydrogen bonding interactions of both solid forms and API are presented in Figure 2.8. The highly polar O···H interaction constitutes 29.7% in Form-II, whereas it is 27.3% for Form-I. However, the contribution of relatively less polar interactions (N···H, S···H, and C···H) are slightly higher in Form-I than that of Form-II, indicating Form-II is more polar than Form-I. The difference in the polarity between the two solid forms may lead to variations in the physicochemical properties such as solubility, permeability, bioavailability, etc. Form-II is expected to have better solubility, but a slower permeability rate than Form-I.

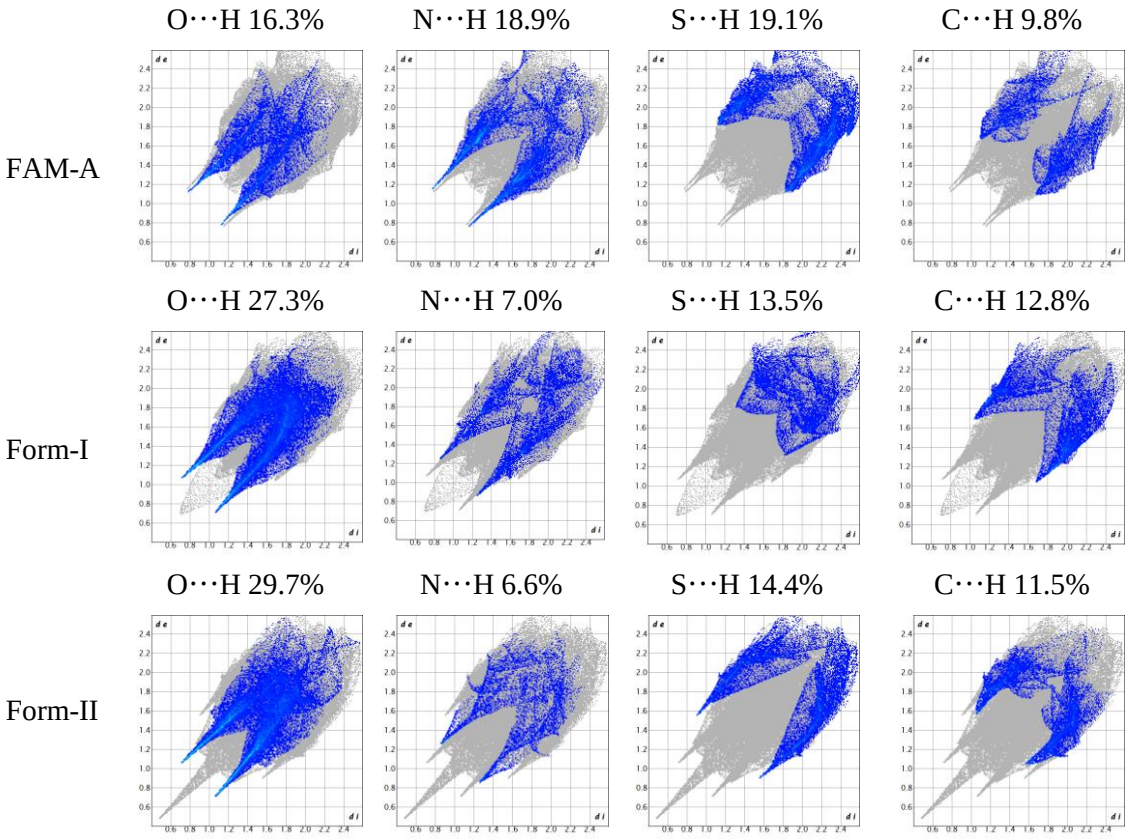

Figure 2.8. 2D fingerprint plots and percentage contribution of various intermolecular interactions of Form-I and Form-II comparison with pure FAM-A.

Apart from the intermolecular interactions, the variation between the dimorphic forms also arises from the voids in their crystal structures. The plots of crystal voids for the two forms of salt are generated in Crystal Explorer version 21 and depicted in Figure 2.9. The voids present in the crystals are calculated using Mercury4.1 linked with Cambridge Structural Data (CSD version 5.43 May 2022 updates). The percentage of voids in the crystal of Form-I is 30.8%, whereas for Form-II is 28.6%.

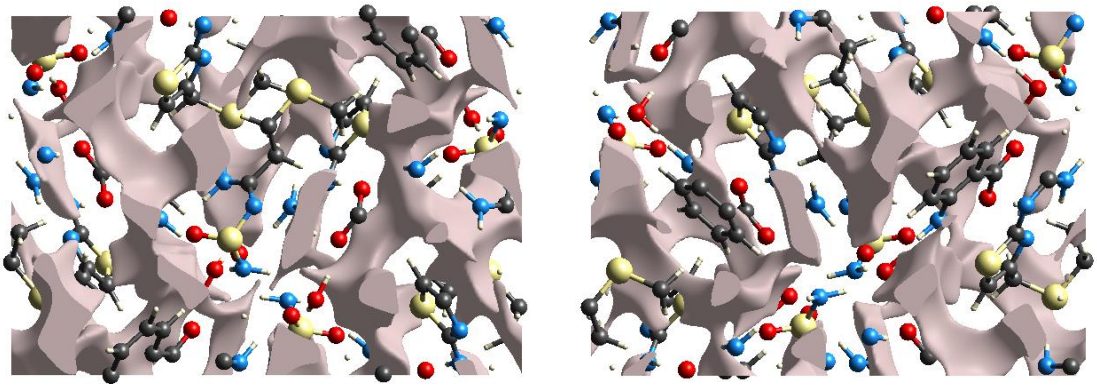

(a) (b)

Figure 2.9 Crystal voids of (a) Form-I and (b) Form-II view along the *a*-axis.

Energy frameworks. The energy frameworks help to visualize the interaction topology and offer insights into both distribution and magnitude of intermolecular interactions [32]. The energy frameworks analysis is carried out for dimorphic forms and the results are available in Figures 2.10 (Form-I) and 2.11 (Form-II). The figures exhibit the electrostatic and dispersion energy contribution to the total energy of each form of the salt. The thickness of each cylinder in the energy frameworks shows the intermolecular interaction strength. The contributions of these intermolecular interaction energies to the total energy of the system have been computed using the *PIXEL* method [33]. The results are available in Table 2.2. The total energy of Form-I (−134.2 kJ mol^{-1}) is higher than that of Form-II (−117.0 kJ mol^{-1}), confirming Form-I is a thermodynamically favored polymorph.

Table 2.2. Estimated energy of various intermolecular interactions in Form-I and Form-II

Solid form	Form-I	Form-II
Electrostatic energy (kJ mol^{-1})	−71.3	−50.9
Polarization energy (kJ mol^{-1})	−33.3	−40.2
Dispersion energy (kJ mol^{-1})	−82.8	−91.3
Repulsion energy (kJ mol^{-1})	61.3	74.5
Total energy (kJ mol^{-1})	−134.2	−117.0

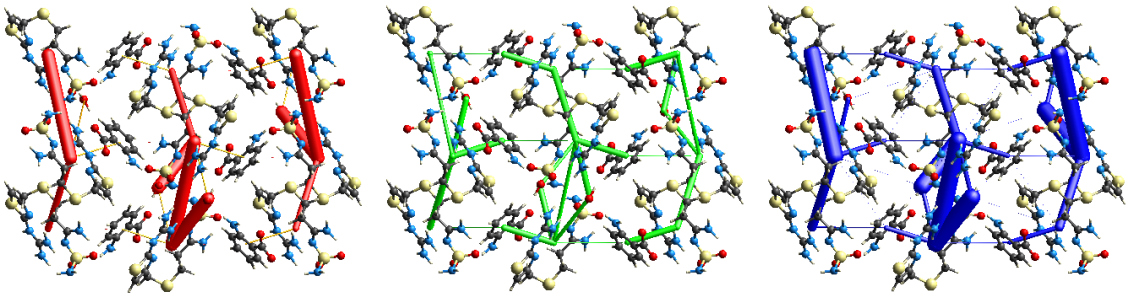

(a) (b) (c)

Figure 2.10 Energy frameworks for Form-I with an energy cutoff at −10 kJ mol^{-1} along the crystallographic *a*-axis. (a) Electrostatic energy (red framework), (b) Dispersion energy (green framework), and (c) Total energy (purple framework).

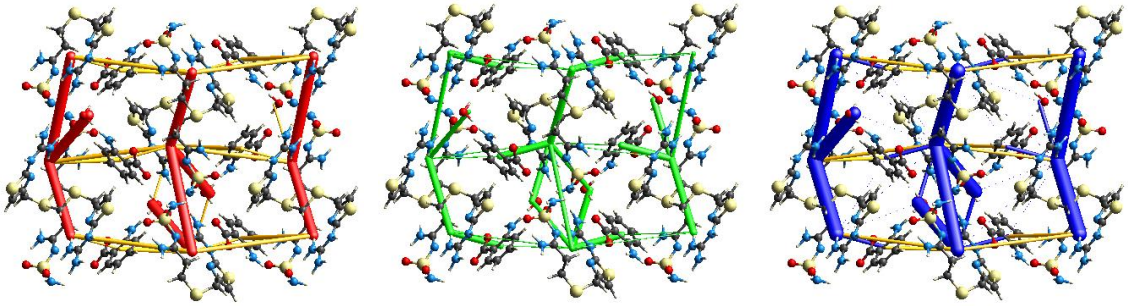

(a) (b) (c)

Figure 2.11 Energy frameworks for Form-II with an energy cutoff at −10 kJ mol^{-1} along the crystallographic *a*-axis. (a) Electrostatic energy (red framework), (b) Dispersion energy (green framework), (c) Total energy (purple framework).

2.3.3 Phase Stability

Because of the chemical degradation of FAM in highly acidic conditions, the phase stability of dimorphic salts was evaluated by doing slurry experiments in acidic media. Excess amounts of the samples were stirred in 1.2 and 7.4 pH buffer solutions for 24 h. The solid phases extracted from the slurries were studied by PXRD. Form-I was found to be stable for up to 24 h in both media, but Form-II started to convert to Form-I (Figure 2.12). Apart from that grinding of Form-II crystals to get the powder material induced polymorphic phase transformation into Form-I which indicates Form-I is thermodynamically more stable than Form-II. The melting points of the two forms also support the better stability of Form-I (Figure 2.2). However, both crystal density and packing fraction of Form-I are lower than that of Form-II which is uncommon for stable polymorph (Form-I: 1.480, 69.2 and Form-II: 1.543 g cm^{-3}; 71.4%) [34,35].

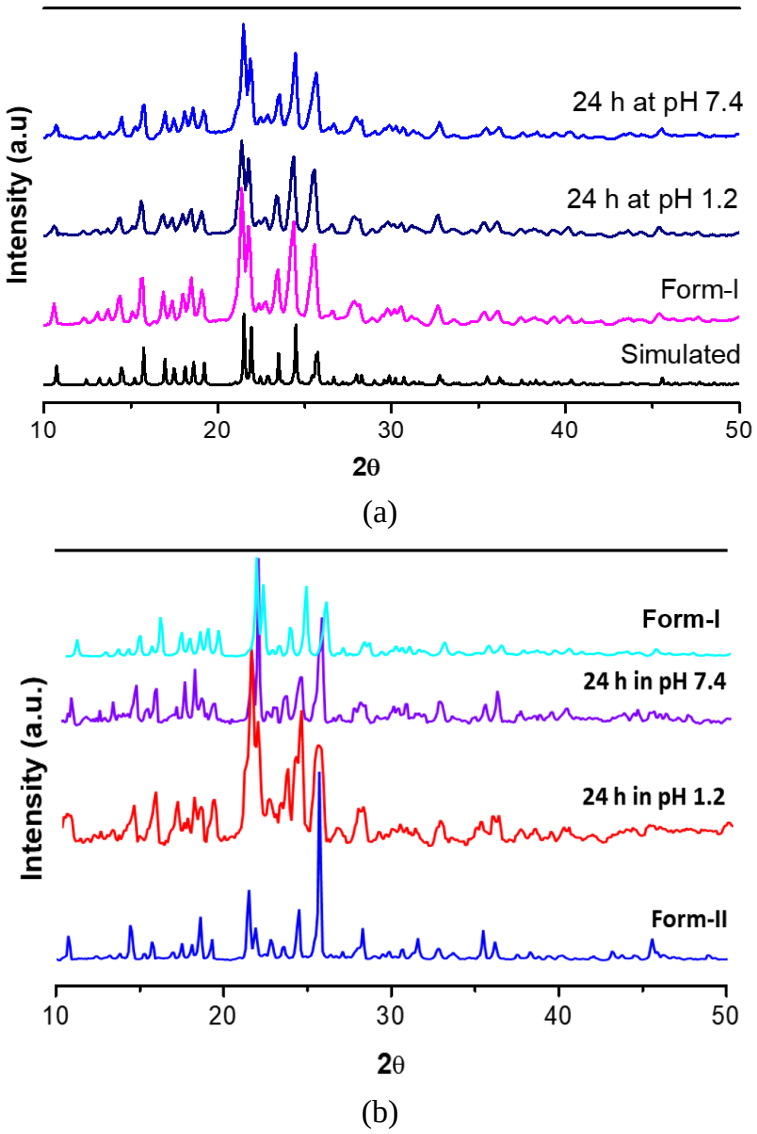

Figure 2.12 Comparison of PXRD profiles of (a) Form-I and (b) Form-II extracted from the slurry experiments in 1.2 and 7.4 pH buffer solutions with the PXRD patterns of respective initial product materials.

2.3.4 Solubility Measurement

It is known that polymorphism in multicomponent solids has an impact on the solubility of pharmaceutical compounds [14]. The solubility and permeability of the obtained two polymorphs were determined in two pH conditions, i.e., simulated gastric and intestinal fluid. The solubility data are plotted in Figure 2.13. The solubility of the two polymorphs is compared with the parent API and found that only Form-II shows a higher solubility than pure FAM at pH 1.2. But at pH 7.4, the solubility of Form-I (4.53 mg/mL) and Form-II (18.13 mg/mL) is 1.8 and 6.8 times higher than that of the parent drug respectively. In both pH conditions, the solubility parameter for Form-II is higher than that of Form-I.

Polar crystalline materials generally demonstrate high solute–solvent interaction with the polar media and display better solubility. The Hirshfeld surface analysis of those dimorphic products reveals that Form-II is more polar than Form-I (Figure 2.8). Thus, the solubility trend is in good agreement with the polarity of the polymorphs. Apart from that thermodynamically less stable solid materials generally display higher solubility. The phase transformation of Form-II into Form-I during grinding suggests that Form-II is thermodynamically less stable than Form-I which can be one of the possible reasons for the better solubility of Form-II. The energy values of different hydrogen bond synthons are responsible for the variation of thermodynamic stability between the two products (Table 2.2).

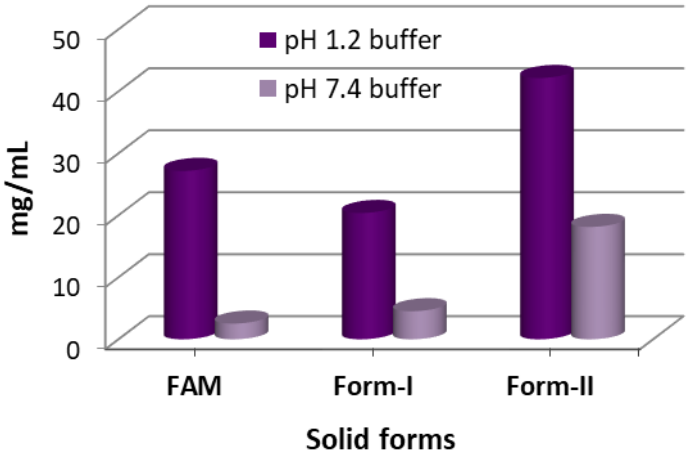

Figure 2.13. The solubility comparison of FAM and its dimorphic salts in a buffer solution of pH 1.2 and 7.4.

2.3.5 Synthon Energy Calculation

Higher interaction energy values between the functional groups of the drug and coformer can certainly indicate the probability of the formation of a stable multicomponent solid. The hydrogen bond geometry analysis in Table 2.1 shows that hydrogen bonding between the guanidine group of the drug and acid group of the coformer for Form-II (bond length =1.77 Å and bond angle = 163°) is weaker and less directional than that of Form-I (bond length = 1.67 Å and bond angle = 174°). The energy of prime hydrogen bond synthon (Figure 2.14a) and hydrogen bonds accessible from the water molecule of crystallization (Figure 2.14b and c) are calculated using Gaussian 09 (B3LYP/6-311G*(d,p). The synthon energy of the prime hydrogen bond in Form-II is found to be lower than that of Form-I by −2.4 kcal mol^{-1} (Figure 2.14a). The synthon energies of hydrogen bonds accessible from the water molecule of crystallization in Form-II (E = −10.2 kcal mol^{-1}) is also found to be

lower than that of the Form-I (E = –22.3 kcal mol^{-1}) by –12.1 kcal mol^{-1} (Figure 2.14b and c). The lower energy values and less directionality of hydrogen bonds for Form-II suggest that it is thermodynamically less stable than Form-I, which explains the better solubility of Form-II. Besides that, the plot of DSC melting endotherms of the two polymorphs in Figure 2.2 shows that the melting point of Form-II (116 °C) is lower than that of Form-I (130 °C). This indicates Form-II has a lower lattice energy than Form-I which also supports the better solubility of Form-II.

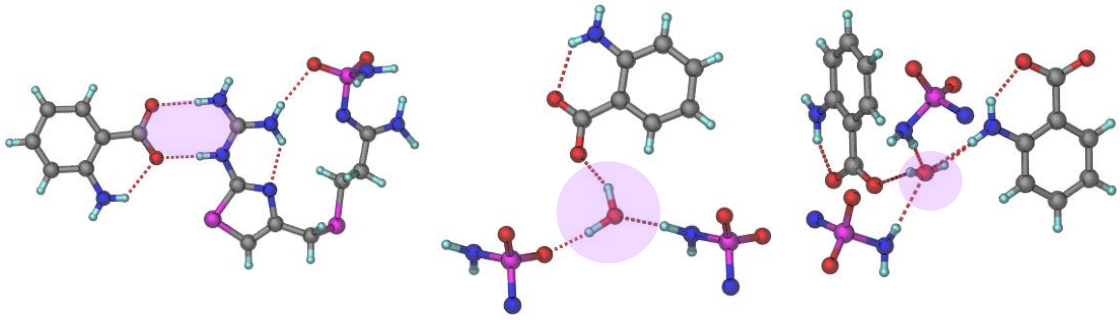

(a) $R_2^2(8)$ motif (b) Form-I (c) Form-II

Figure 2.14. (a) The main structural $R_2^2(8)$ motif is common in both crystalline forms. (b) and (c)The water molecule of crystallization in Form-II forms a higher number of hydrogen bonds with the drug and coformer, but those bonds are found to be weaker than that of Form-I.

2.3.6 Membrane Permeation Behaviour

The overall bioavailability of oral drugs depends on the amount of drug material permits through the cell membrane. The permeation rate and amount of drug flux for Form-I and Form-II are measured and compared with the pure API. These parameters are determined in the simulated intestinal pH condition, i.e., pH 7.4 using nitrocellulose membrane and the results are plotted in Figure 2.15. The plot demonstrates that the permeation rate of Form-I is higher than the parent API. The permeation rate of Form-II is lower up to 60 min, but gradually increases and displays a higher rate than that of the pure drug (Figure 2.15a). The maximum drug flux was observed at 5 min for the pure FAM and its salt polymorphs (Form-I and Form-II). Form-I shows a higher density of drug flux than pure FAM, whereas the amount of drug flux is lower for Form-II (Figure 2.15b). Highly polar drug molecules generally display poor permeation behaviors because of the low partition coefficient in polar media, i.e., low lipophilicity [36]. The Hirshfeld surface analysis in Figure 2.8 shows that the lipophilic nature of Form-II is lower than that of Form-I which might be one of the reasons for the lower permeability of Form-II.

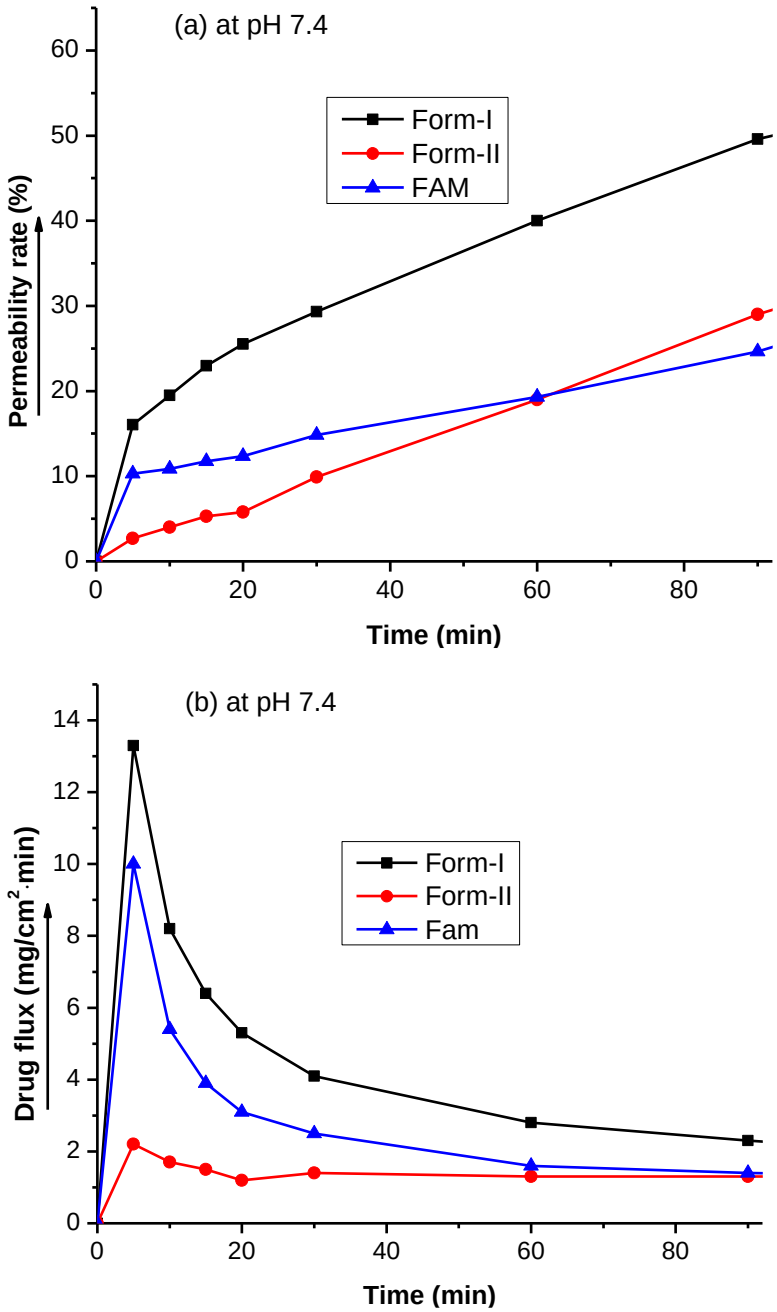

Figure 2.15. (a) Permeability rate and (b) drug flux of FAM and its dimorphic salts with respect to time.

2.4 Summary

Two polymorphic phases of molecular salt hydrate of the anti-ulcer drug famotidine with *ortho*-aminobenzoic acid were isolated, characterized, and reported unalike properties. Though the drug conformations are overlaid with each other, the topological distributions for N–H···O and O–H···O hydrogen bonding interactions are discrete. Such hydrogen bonds mostly differ at the site accessible from the water molecule of crystallization and are detected as the key reason for modulating drug efficacy. The noticeable differences in

the orientation of the water molecule of crystallization lead to disparity in the intermolecular interactions and eventually the drug property. The qualitative and quantitative contribution of these weak interactions corroborated with the accessed solubility and membrane permeation properties by the two forms at physiological pH environments. The distributions for N–H···O and O–H···O along with supported other hydrogen bonds, and solute-solvent interactions have revealed immense influences on the drug property in multicomponent polymorphic crystals. This study offers an understanding of the accountable reasons that essentially result from the disparity in properties with IP coverage in a closely related dimorphic multicomponent system.

2.5 Experimental Section

2.5.1 Materials

Famotidine (purity ~99%) and 2-ABA were bought from Yarrow chem products and Sigma-Aldrich, India respectively, and used as received. Solvents (methanol and ethanol, HPLC-grade) used for crystallization were purchased from SRL, India. Solubility and permeability parameters measurement was done using Millipore water.

2.5.2 Synthesis of Dimorphic Molecular Salt Hydrates

1 mmol of each starting material was taken in a mortar and ground with the addition of 3-4 drops of water for 30 min. Single crystals of Form-I and II were obtained from the crystallization of ground material in methanol and ethanol respectively. The crystallization was carried out by slow evaporation of solvent at room temperature.

2.5.3 Vibrational Spectroscopy (FT-IR)

The IR spectra were recorded on a PerkinElmer Frontier MIR FTIR spectrophotometer in the range of 450–4000 cm^{-1} (Figure 2.1).

2.5.4 Differential Scanning Calorimetry (DSC)

DSC melting thermograms of the polymorphs were measured in the range of 25–250 °C on Mettler Toledo DSC 822e. Around 10 mg of the products were used to collect the data. The endothermic melting temperature of the polymorphs of the salt was compared with the API and found to be different from it (Figure 2.2).

2.5.5 Thermogravimetric Analysis (TGA)

The Mettler Toledo TGA/SDTA 851e module was used to evaluate the quantity of lattice solvent molecules that are presented in the molecular salts. 5–7 mg of the products were placed in an alumina pan and heated in the range of 30–300 °C at a 10 °C/min rate under a dry nitrogen flow of 30 mL/min (Figure 2.3).

2.5.6 Powder X-ray Diffraction (PXRD)

PXRD data of the samples were collected on a Bruker X-ray diffractometer with Cu-Kα X-radiation (λ = 1.54056 Å). The recording was performed in the 2θ of 10–40° range at a scanning rate of 1° min^{-1}. The phase purity of the polymorphs was confirmed using Rietveld refinement and is available in Appendix Figure A1.

2.5.7 Single Crystal X-ray Diffraction (Single crystal X-RD)

Single crystal X-RD data of Form-I and Form-II were collected on Bruker SMART APEX-II CCD diffractometer using Mo Kα radiation of λ = 0.71073 Å. Data reduction and correction of absorption intensity were carried out using Bruker SAINT Software and SADABS respectively [37]. The refinement of data of both polymorphs was performed using SHELXL[38]. The packing diagrams were plotted using X-Seed [39]. The summary of the crystallographic data for Form-I and Form-II is available in Appendix Table A1. Hydrogen bond geometry is listed in Table 2.1.

2.5.8 Hirshfeld Surface Analysis and Energy Frameworks

The contribution percentage of various intermolecular interactions and energy frameworks of the dimorphic salt hydrates were calculated using Crystal Explorer version 21 at the B3LYP/6-31G *(d, p) level of theory and cutoff radius 3.8 Å of the reference molecule (Figures 2.8-11) [32]. The calculation of the overall energy framework consists of electrostatic, polarization, dispersion, and repulsion parameters with 1.057, 0.740, 0.871, and 0.618 as base scales, respectively [40].

2.5.9 DFT Calculation

The energy values of the hydrogen-bonded synthons in the crystal structure of the two polymorphs of the molecular salt were computed using Gaussian09 on DFT with B3LYP; 6311G *(d, p) as the basic level (Figure 2.14).

2.5.10 Cambridge Structural Database (CSD)

The CSD survey was carried out with the latest version, CSD 2023.1 software coupled with Mercury 4.2.0. An overlay of drug and 2-ABA conformers extracted from the crystal structures of the dimorphic molecular salts was drawn on Mercury4.2 linked to Cambridge Structural Data (Figure 2.7).

2.5.11 Solubility Measurements

The solubility of Form-I and Form-II and drug FAM was measured by UV–visible spectroscopy in the buffer solution of pH 1.2 and 7.4 (Figure 2.13). An excess quantity of the samples of these materials was dissolved in 3 mL of 1.2 pH saline buffer and 7.4 pH phosphate buffer and stirred at a rate of 800 rpm at ambient temperature for 12 h. The measurement was done three times to make sure the consistency of the results. The absorbance of the filtered solution was recorded in an Agilent Carry-60 UV–visible double beam spectrophotometer. The unknown concentration (C_u) of each polymorph sample was computed from the calibration curve's equation $C_u = (A_u - \text{intercept})/\text{slope}$, where A_u is the absorbance of the unknown sample.

2.5.12 Membrane Permeability

The amount of drug permits across the nitrocellulose membrane was studied using a diffusion apparatus following the procedure reported in the literature [36,41,42]. A donor compartment was prepared with 5 mg of sample in the membrane and closed with a clip and placed in the receptor compartment containing a 100 mL buffer solution pH 7.4. The solution was allowed to stir at the rate of 800 rpm at a room temperature of 25 °C. Three milliliters of the solution were withdrawn from the receptor compartment at the time interval of 5, 10, 15, 20, 30, 60, and 90 min. The receptor compartment's solution volume was kept constant by adding an equal amount of fresh solution in each interval. The amount of the drug permitted across the membrane was analyzed by UV–vis spectrophotometry. The permeability rate and the quantity of drug flux at a pH 7.4 medium are plotted in Figure 2.15.

2.6 References

[1] Yousef, M. A. E. and Vangala, V. R. Pharmaceutical cocrystals: Molecules, crystals, formulations, medicines. *Crystal Growth & Design*, 19(12):7420-7438, 2019.

[2] Saikia, B., Pathak, D., and Sarma, B. Variable stoichiometry cocrystals: occurrence and significance. *CrystEngComm*, 23(26):4583-4606, 2021.

[3] Kavanagh, O. N., Croker, D. M., Walker, G. M., and Zaworotko, M. J. Pharmaceutical cocrystals: from serendipity to design to application. *Drug Discovery Today*, 24(3):796-804, 2019.

[4] Thakuria, R. and Sarma, B. Drug-drug and drug-nutraceutical cocrystal/salt as an alternative medicine for combination therapy: a crystal engineering approach. *Crystals*, 8(2):101, 2018.

[5] Shan, N. and Zaworotko, M. J. The role of cocrystals in pharmaceutical science. *Drug discovery today*, 13(9-10):440-446, 2008.

[6] Chen, J., Sarma, B., Evans, J. M. B., and Myerson, A. S. Pharmaceutical crystallization. *Crystal growth & design*, 11(4):887-895, 2011.

[7] Jones, W., Motherwell, W. D. S., and Trask, A. V. Pharmaceutical cocrystals: An emerging approach to physical property enhancement. *MRS bulletin*, 31(11):875-879, 2006.

[8] Sarma, B. and Saikia, B. Hydrogen bond synthon competition in the stabilization of theophylline cocrystals. *CrystEngComm*, 16(22):4753-4765, 2014.

[9] Saikia, B., Bora, P., Khatioda, R., and Sarma, B. Hydrogen Bond Synthons in the Interplay of Solubility and Membrane Permeability/Diffusion in Variable Stoichiometry Drug Cocrystals. *Crystal Growth and Design*, 15(11):5593-5603, 2015.

[10] Steed, J. W. The role of co-crystals in pharmaceutical design. *Trends in pharmacological sciences*, 34(3):185-193, 2013.

[11] Etter, M. C. and Reutzel, S. M. Hydrogen bond directed cocrystallization and molecular recognition properties of acyclic imides. *Journal of the American Chemical Society*, 113(7):2586-2598, 1991.

[12] Desiraju, G. R. Supramolecular synthons in crystal engineering—a new organic synthesis. *Angewandte Chemie International Edition in English*, 34(21):2311-2327, 1995.

[13] Bolla, G., Sarma, B., and Nangia, A. K. Crystal Engineering of Pharmaceutical Cocrystals in the Discovery and Development of Improved Drugs. *Chemical Reviews*, 122(13):11514–11603, 2022.

[14] Aitipamula, S., Chow, P. S., and Tan, R. B. H. Polymorphism in cocrystals: a review and assessment of its significance. *CrystEngComm*, 16(17):3451-3465, 2014.

[15] Khatioda, R., Bora, P., and Sarma, B. Trimorphic ethenzamide cocrystal: in vitro solubility and membrane efflux studies. *Crystal Growth & Design*, 18(8):4637-4645, 2018.

[16] Goud, N. R. and Nangia, A. Synthon polymorphs of sulfacetamide–acetamide cocrystal based on N–H⋯ O [double bond, length as m-dash] S and N–H⋯ O [double bond, length as m-dash] C hydrogen bonding. *CrystEngComm*, 15(37):7456-7461, 2013.

[17] Aitipamula, S., Chow, P. S., and Tan, R. B. H. Trimorphs of a pharmaceutical cocrystal involving two active pharmaceutical ingredients: potential relevance to combination drugs. *CrystEngComm*, 11(9):1823-1827, 2009.

[18] Trask, A. V, Motherwell, W. D. S., and Jones, W. Pharmaceutical cocrystallization: engineering a remedy for caffeine hydration. *Crystal Growth & Design*, 5(3):1013-1021, 2005.

[19] Bora, P., Pathak, D., Kalita, B. K., and Sarma, B. Deciphering the Role of Environmental Variables in the Nucleation of Stoichiometric Cocrystals. *Crystal Growth & Design*, 23(3):1500-1510, 2023.

[20] Bezerra, B. P., Pogoda, D., Perry, M. L., Vidal, L. M. T., Zaworotko, M. J., and Ayala, A. P. Cocrystal polymorphs and solvates of the anti-trypanosoma cruzi drug benznidazole with improved dissolution performance. *Crystal Growth & Design*, 20(7):4707-4718, 2020.

[21] Ghosh, S., Mondal, A., Kiran, M., Ramamurty, U., and Reddy, C. M. The role of weak interactions in the phase transition and distinct mechanical behavior of two structurally similar caffeine co-crystal polymorphs studied by nanoindentation. *Crystal growth & design*, 13(10):4435-4441, 2013.

[22] Beloborodova, A. A., Minkov, V. S., Rychkov, D. A., Rybalova, T. V, and Boldyreva, E. V. First evidence of polymorphism in furosemide solvates. *Crystal Growth & Design*, 17(5):2333-2341, 2017.

[23] Davey, R. J. Polymorphism in Molecular Crystals Joel Bernstein. Oxford University Press, New York, 2002. ISBN 0198506058. 20022002.

[24] Kersten, K., Kaur, R., and Matzger, A. Survey and analysis of crystal polymorphism in organic structures. *IUCrJ*, 5(2):124-129, 2018.

[25] Golic, L., Djinovic, K., and Florjanic, M. Structure of a new crystalline form of famotidine. *Acta Crystallographica Section C*, 45(9):1381-1384, 1989.

[26] Shankland, K., McBride, L., David, W. I. F., Shankland, N., and Steele, G.

Molecular, crystallographic and algorithmic factors in structure determination from powder diffraction data by simulated annealing. *Journal of Applied Crystallography*, 35(4):443-454, 2002.

[27] Saikia, B., Sultana, N., Kaushik, T., and Sarma, B. Engineering a Remedy to Improve Phase Stability of Famotidine under Physiological pH Environments. *Crystal Growth and Design*, 19(11):6472-6481, 2019.

[28] McKinnon, J. J., Fabbiani, F. P. A., and Spackman, M. A. Comparison of Polymorphic Molecular Crystal Structures through Hirshfeld Surface Analysis. *Crystal Growth & Design*, 7(4):755-769, 2007.

[29] Bergantin, S. and Moret, M. Rubrene Polymorphs and Derivatives: The Effect of Chemical Modification on the Crystal Structure. *Crystal Growth & Design*, 12(12):6035-6041, 2012.

[30] Rohl, A. L., Moret, M., Kaminsky, W., Claborn, K., McKinnon, J. J., and Kahr, B. Hirshfeld surfaces identify inadequacies in computations of intermolecular interactions in crystals: pentamorphic 1, 8-dihydroxyanthraquinone. *Crystal Growth and Design*, 8(12):4517-4525, 2008.

[31] Carter, D. J., Raiteri, P., Barnard, K. R., Gielink, R., Mocerino, M., Skelton, B. W., Vaughan, J. G., Ogden, M. I., and Rohl, A. L. Difference Hirshfeld fingerprint plots: a tool for studying polymorphs. *CrystEngComm*, 19(16):2207-2215, 2017.

[32] Turner, M. J., Thomas, S. P., Shi, M. W., Jayatilaka, D., and Spackman, M. A. Energy frameworks: insights into interaction anisotropy and the mechanical properties of molecular crystals. *Chemical Communications*, 51(18):3735-3738, 2015.

[33] Gavezzotti, A. Efficient computer modeling of organic materials. The atom–atom, Coulomb–London–Pauli (AA-CLP) model for intermolecular electrostatic-polarization, dispersion and repulsion energies. *New Journal of Chemistry*, 35(7):1360-1368, 2011.

[34] Aitipamula, S., Chow, P. S., and Tan, R. B. H. Trimorphs of a pharmaceutical cocrystal involving two active pharmaceutical ingredients: potential relevance to combination drugs. *CrystEngComm*, 11(9):1823-1827, 2009.

[35] Thallapally, P. K., Jetti, R. K. R., Katz, A. K., Carrell, H. L., Singh, K., Lahiri, K., Kotha, S., Boese, R., and Desiraju, G. R. Polymorphism of 1, 3, 5-trinitrobenzene induced by a trisindane additive. *Angewandte Chemie International Edition*, 43(9):1149-1155, 2004.

[36] Sanphui, P., Devi, V. K., Clara, D., Malviya, N., Ganguly, S., and Desiraju, G. R. Cocrystals of Hydrochlorothiazide: Solubility and Diffusion/Permeability Enhancements through Drug–Coformer Interactions. *Molecular Pharmaceutics*, 12(5):1615-1622, 2015.

[37] SAINT Plus (v 6.14); Bruker AXS Inc. Inc., Madison, WI,. 20082008.

[38] Madison, A. I. :W. Inc., Madison, WI,. 20082008.

[39] Barbour, L. J. X-Seed, graphical interface to SHELX-97 and POV-Ray. *University of Missouri-Columbia, Columbia, MO*, 19991999.

[40] Thomas, S. P., Spackman, P. R., Jayatilaka, D., and Spackman, M. A. Accurate lattice energies for molecular crystals from experimental crystal structures. *Journal of Chemical Theory and Computation*, 14(3):1614-1623, 2018.

[41] Bora, P., Saikia, B., and Sarma, B. Regulation of π···π Stacking Interactions in Small Molecule Cocrystals and/or Salts for Physiochemical Property Modulation. *Crystal Growth & Design*, 18(3):1448-1458, 2018.

[42] Khatioda, R., Saikia, B., Das, P. J., and Sarma, B. Solubility and in vitro drug permeation behavior of ethenzamide cocrystals regulated in physiological pH environments. *CrystEngComm*, 19(46):6992-7000, 2017.